ISEIS

Journal of Environmental Informatics 39(2) 111-124 (2022)

Journal of Environmental Informatics

www.iseis.org/jei

Development of A Simulation-Based Multi-Objective Optimization Method for Improving the Advanced Oxidizing Capacity of Hydrodynamic Cavitation Reactor - A Case Study of Self-Excited Oscillation Cavity

S. L. Nie[1], J. K. Zhou[1], H. Ji[1 *], Z. Y. Dai[2], and Z. H. Ma[1]

[1] *Beijing Key Laboratory of Advanced Manufacturing Technology, Beijing University of Technology, Beijing 100124, China*
[2] *Hubei Key Laboratory of Critical Zone Evolution, China University of Geosciences, Wuhan, Hubei 430074, China*

Received 26 July 2021; revised 18 November 2021; accepted 14 December 2021; published online 18 January 2022

ABSTRACT. In this study, a simulation-based multi-objective optimization method is developed for optimizing the structural design of hydrodynamic cavitation (HC) reactor and improving the cavitation effect of HC reactor. The developed method integrates simulation technique of computational fluid dynamics (CFD) and optimization techniques of surrogate model and nondominated sorting genetic algorithm II (NSGA-II) into a general framework. The effect of structure parameters and their interactions on the cavitation effect of the self-excited oscillation cavity (SEOC) are analyzed. Results demonstrate that optimization techniques of surrogate model and NSGA-II can effectively improve the structure and the capacity of SEOC. Simulation results show that the internal vapor volume fraction and outlet vapor volume fraction of SEOC (based on the optimized structure) increase by 13.46 and 38.01%, respectively. The optimized structure of SEOC is also verified experimentally through the degradation experiment of methylene blue solution. The degrees of degradation before and after optimization respectively are 10.12 and 16.14%, and the degradation capacity increases by 59.5%. This study will play a significantly guiding role on the optimization design of HC reactor for advanced oxidation processes (AOPs) to obtain the preferable cavitation effect.

Keywords: AOPs, CFD simulation, hydrodynamic cavitation, multi-objective optimization, self-excited oscillation cavity, surrogate model

1. Introduction

With the progress of modern society and the rapid development of industry, a large amount of wastewater containing organic matter is produced, making the problem of water pollution increasingly serious (Sun et al., 2020a). Organic pollutants in wastewater, such as ammonia nitrogen, will deteriorate water quality, lead to eutrophication of water, and cause serious environmental problems. At the same time, the composition of organic pollutants in wastewater is complex, which is generally poisonous and carcinogenic to living organisms (Rajoriya et al., 2017). Therefore, wastewater treatment measures have received more and more attention.

A number of methods based on physical, biological and advanced oxidation processes (AOPs) can effectively treat organic wastewater (Asztalos and Kim, 2017; Yi et al., 2018). AOPs possess strong oxidation capacity, which can produce hydroxyl radicals (·OH) through physical and chemical processes. It can also react with most organic pollutants in a fast chain, and convert harmful substances into carbon dioxide (CO_2), H_2O, and mineral salts without secondary pollution. AOPs include a various of processes such as ozone, Fenton, ultrasonic cavitation, hydrodynamic cavitation (HC), etc (Bhat and Gogate, 2020). HC can reduce the local pressure of the fluid flowing through the structure below the saturated vapor pressure, at which time the cavitation bubbles appear in the liquid. In the cavitation process, the bubble undergoes three stages of formation, growth, and collapse; in the collapse process, the bubble produces a series of physical and chemical effects, thereby generating a large number of hydroxyl radicals (·OH) (Franke et al., 2011). Previously, a number of researchers demonstrated that the HC and its combination with other oxidation methods have significant positive effects on the degradation of industrial wastewater, Salicylic acid, Rhodamine B, carbamazepine, imidacloprid, petroleum refinery effluent and benzene present in wastewater (Chakinala et al., 2009; Mishra and Gogate, 2010; Patil et al., 2014; Thanekar et al., 2018; Doltade et al., 2019; Thanekar et al., 2021). Recently, as one of novel AOPs, HC has attracted much attention in the field of wastewater treatment (especially refractory wastewater), featured by fast reaction rate, strong oxidation capacity, low-cost operating, green, and non-pollution, as well as simple equipment, large treatment capacity and easy combination with other techniques (Gogate, 2020).

Several scholars have demonstrated the effectiveness and applicability of the self-excited oscillation cavity (SEOC). Ge-

* Corresponding author: Tel: +86 1067396362; fax: +86 1067391617.
E-mail address: jihui@bjut.edu.cn (H. Ji).

ISSN: 1726-2135 print/1684-8799 online
 doi:10.3808/jei.202200474.

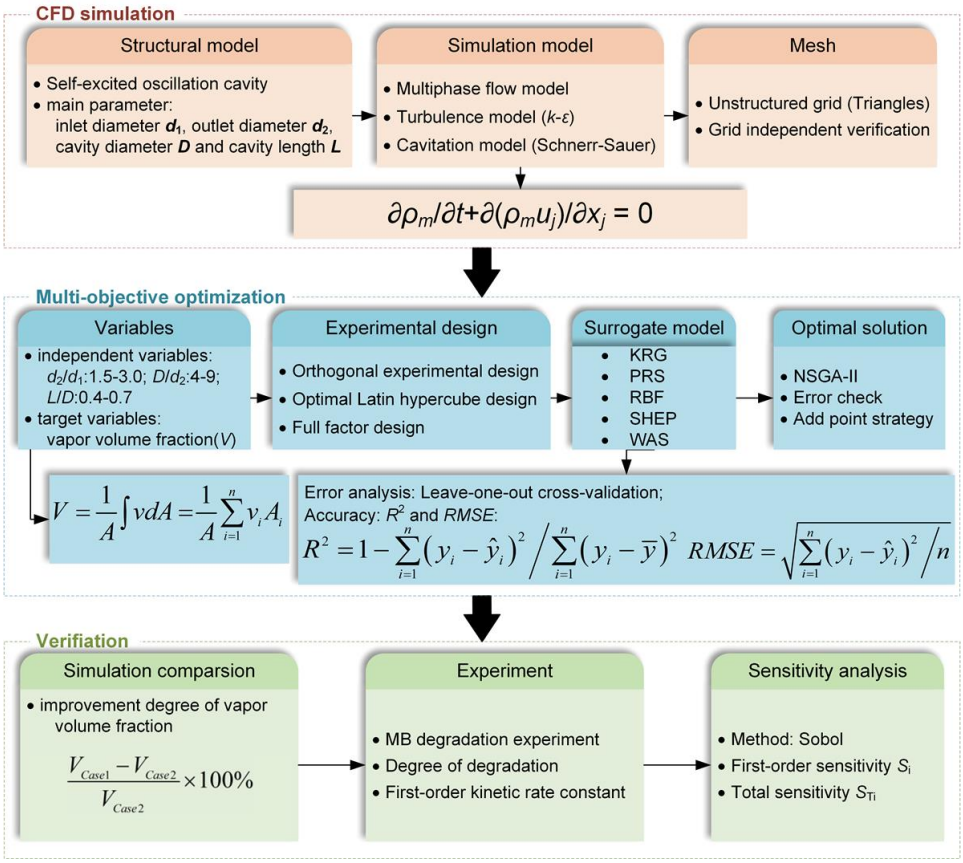

Figure 1. Research scheme.

veci et al. (2003) analyzed the effective wavelength of the SEOC and the phase velocity of the vortex structure, which could provide guidance for the optimization of nozzle structure parameters and the physical model of the dimensionless frequency of oscillation. Li et al. (2016) analyzed the effect of nozzle inlet area discontinuity on axial pressure oscillation on the basis of previous related studies, and conducted an experimental study using Helmholtz nozzles. The study found that the area discontinuity could increase the pressure oscillation amplitude, and had almost little effect on the oscillation frequency. Zhou et al. (2017) conducted experimental studies on the flow field characteristics and pressure oscillation characteristics of pulsed jets, and studied the influence of bubble clouds in SEOC with pump pressure and confining pressure. Wang et al. (2019) optimized the cavity diameter, outlet diameter and working pressure of the SEOC through response surface model and computational fluid dynamics to improve the spray quality of the nozzle. Xiang et al. (2020) analyzed the periodic dynamic characteristics of the pulsed cavitation jet under the best experimental conditions, and explained the generation mechanism of the cavitation jet. Fang et al. (2020) proved that there is a close relationship between the vortex-cavitation interaction and the flow mechanism in the Helmholtz oscillator through numerical simulations.

Generally, the cavitation generated in SEOC determines the effect of HC in the degradation of wastewater. The working principles and flow field characteristics of SEOC provide theoretical guidance for the structural design of SEOC. Unfortunately, few studies focus on the structural optimization design method to achieve the better cavitation effect for SEOC. Univariate optimization based on control variables and orthogonal experiment optimization are two common SEOC structural optimization methods (Wang, 2005; Jin and Mi, 2016; Zhang et al., 2021). However, univariate optimization ignores the interaction between the parameters, leading to the result fall into the local optimum. Although the orthogonal experiment optimization method considers the interaction between the parameters, the result is often just a combination the level of factor sets, which can cause the optimal structural parameters to be inaccurate.

Therefore, this study aims to develop a simulation based multi-objective optimization method for optimizing the structure of SEOC, which incorporates techniques of computational fluid dynamics (CFD) simulation, surrogate model, and non-dominated sorting genetic algorithm II (NSGA-Ⅱ) within a general framework. The main research components of this study can be summarized as follows: (i) a simulation-based multi-objective optimization method is developed for improv-ing the advanced oxidizing capacity of HC reactor; (ii) CFD simulation is used for predicting the cavitation capacity of HC reactor and analyzing the influence of various parameters as well as their interactions on the cavitation effect; (iii) surrogate model

and NSGA-II in association with low computation and global optimal solution are capable of optimizing the structure of SEOC; (iv) compared with the conventional univariate and orthogonal experiment optimization method, simulation results and experimental tests demonstrated that the proposed method can increase degradation degree and capacity of HC reactor. Figure 1 shows the scheme of this study.

2. Methodology

2.1. Principle of Cavitation Effect and Degradation Mechanism

Figure 2(a) shows the structure and working principle of SEOC. The main structural parameters are the upper nozzle inlet diameter d_1, the lower nozzle outlet diameter d_2, the cavity diameter D and the cavity length L (Zhou et al., 2017; Wang et al., 2019).

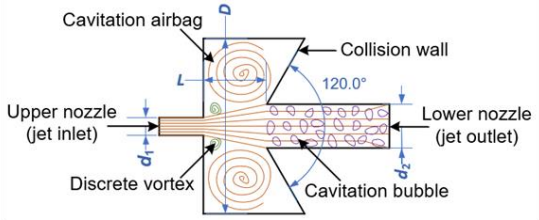

(a) Working principle diagram

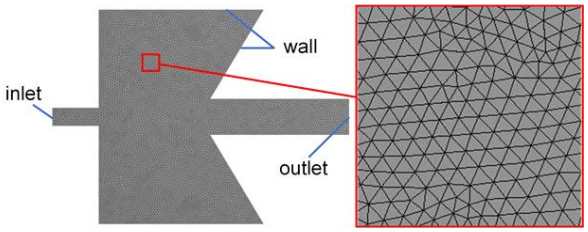

(b) Geometric model meshing

Figure 2. SEOC structure diagram.

When the fluid enters the cavity from the jet inlet (i.e. upper nozzle) of SEOC, the high-speed jet has strong shear with the static liquid in the cavity, which can form a turbulent shear layer in the flow direction of the fluid and generating discrete vortices. The pressure oscillation wave is generated when the discrete vortex interacts with the collision wall. The wave then propagates upward at the speed of sound and triggers a new vortex disturbance. Repeatedly, due to the barrier of the collision wall, the vortex can be further magnified and moved to the center of the cavity, forming a larger vortex. The pressure in the center of the vortex gradually decreases, forms a negative pressure area, generates a large number of cavitation bubbles, and eventually results in cavitation airbag (Wang et al., 2017).

In this process, the mechanism of HC degrades pollutants as shown in Equations (1) and (2). Cavitation bubbles release energy during the collapse process, resulting in a high energy density. The large amount of energy can form local high temperature and pressure (5000 ~ 10000 K and 500 ~ 1000 atm) in a very short time. Under these extreme conditions, water molecules split to produce hydroxyl radicals (Li et al., 2020; Yi et al., 2021). Therefore, under certain working conditions, the cavitation effect has a great impact on the degradation effect.

$$H_2O \xrightarrow{HC} gOH + gH \tag{1}$$

$$\text{Organic pollutants} + gOH \rightarrow CO_2 + H_2O \text{ etc.} \tag{2}$$

2.2. Simulation Modeling for CFD Flow

It is assumed that the mixture of liquid and vapor is uniform and has no slip velocity. The mixture model is used as the calculation model for multiphase flow, the turbulence state is considered, the effect of cavitation is added, and the cavitation control equations are finally formed. The corresponding continuity equation, momentum equation and mass conservation equation of the multiphase flow model are as follows (Huang et al., 2013):

$$\frac{\partial \rho_m}{\partial t} + \frac{\partial \left(\rho_m u_j\right)}{\partial x_j} = 0 \tag{3}$$

$$\frac{\partial \left(\rho_m u_j\right)}{\partial t} + \frac{\partial \left(\rho_m u_i u_j\right)}{\partial x_j} = -\frac{\partial p}{\partial x_i} + \frac{\partial}{\partial x_j}\left[\left(\mu + \mu_t\right)\left(\frac{\partial u_i}{\partial x_j} + \frac{\partial u_j}{\partial x_i} - \frac{2}{3}\frac{\partial u_i}{\partial x_j}\delta_{ij}\right)\right] \tag{4}$$

$$\frac{\partial \rho_l \alpha_l}{\partial t} + \frac{\partial \left(\rho_l \alpha_l u_j\right)}{\partial x_j} = \dot{m}^+ + \dot{m}^- \tag{5}$$

where ρ_m and ρ_l are the density of mixture and liquid respectively, u is the velocity of the mixture, p is the pressure of the mixture, μ is the laminar viscosity of the mixture, μ_t is the turbulent dynamic viscosity of the mixture, α_l is the volume fraction of liquid, $\dot{m}^+$ is the condensation rates, and $\dot{m}^-$ is the evaporation rates.

In this study, CFD fluent is used for numerical calculation. The standard k-ε model is used to describe the turbulence state, and the k-ε equation can be expressed as follows:

$$\frac{\partial \left(\rho x\right)}{\partial t} + \frac{\partial \left(\rho k u_1\right)}{\partial x_i} = \frac{\partial}{\partial x_j}\left[\left(\mu + \frac{\mu_t}{\sigma_k}\right)\frac{\partial k}{\partial x_j}\right] + G_k + G_b - \rho_\varepsilon - Y_M + S_k \tag{6}$$

$$\frac{\partial \left(\rho \varepsilon\right)}{\partial t} + \frac{\partial \left(\rho \varepsilon u_i\right)}{\partial x_i} = \frac{\partial}{\partial x}\left[\left(\mu + \frac{\mu_t}{\sigma_\varepsilon}\right)\frac{\partial \varepsilon}{\partial x_j}\right] + C_{1\varepsilon}\frac{\varepsilon}{k}\left(G_k + C_{3\varepsilon}G_b\right) - C_{2\varepsilon}\frac{\varepsilon^2}{k} + S_\varepsilon \tag{7}$$

where μ is the laminar viscosity coefficient, μ_t is the turbulent viscosity coefficient, G_k is the turbulent kinetic energy generat-

ed by laminar velocity gradient, Y_M is the fluctuation caused by excessive diffusion in compressible turbulence, G_b is the turbulent kinetic energy generated by buoyancy, and $C_{1\varepsilon}$, $C_{2\varepsilon}$, $C_{3\varepsilon}$, σ_k, and σ_ε are constants.

In this study, Schnerr-Sauer cavitation model based on Rayleigh-Plesset equation is used in numerical calculation. The following equations are employed to describe the mass transfer process of vapor and liquid (Sun et al., 2015):

$$R_e = -\frac{\rho_v \rho_l \alpha_v (1-\alpha_v)}{\rho_m} \frac{3}{R_B} \sqrt{\frac{2(p_v - p)}{3\rho_l}}, \; p_v \geq p \tag{8}$$

$$R_c = -\frac{\rho_v \rho_l \alpha_v (1-\alpha_v)}{\rho_m} \frac{3}{R_B} \sqrt{\frac{2(p - p_v)}{3\rho_l}}, \; p_v < p \tag{9}$$

where R_e and R_c represent the process of evaporation and condensation respectively, α_v is local vapor volume fraction, ρ_m is the mixtures density, ρ_v is the vapor density, R_B is the bubble radius, and p_v is the saturated vapor pressure.

The model grid based on the unstructured grid is established as shown in Figure 2(b). In the CFD simulation, liquid water is the primary phase, vapor is the secondary phase, the inlet pressure is 1 MPa, and the outlet pressure is 1 atm. The pressure-based solver is used for steady-state calculations, and the pressure-velocity coupling algorithm is SIMPLEC, with a convergence criterion of residual values below 10^{-3} and stable balance of inlet and outlet flows. In order to eliminate the influence of grid size on the numerical simulation results to ensure the credibility of the results, the grid independence of the numerical model is verified in this study.

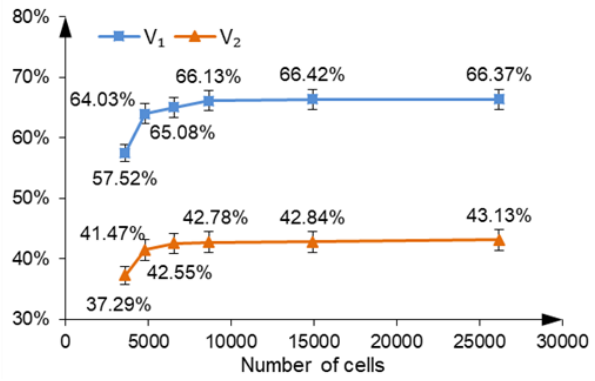

Figure 3. Calculation results of different number of cells.

In order to test the grid independence, the same grid division method is used for generating 6 kinds of grids. The appropriate number of grids is selected through comparing the vapor volume fraction in the cavity and the outlet. Figure 3 presents the calculation results of different number of cells, where V_1 is the area-weighted average vapor volume fraction in the cavity and V_2 is the weighted average vapor volume fraction at the outlet. As shown in Figure 3, with the increase of the number of cells, the calculation results increase firstly, and then tend to be stable. When the number of cells exceeds 15000, the change rates of V_1 and V_2 are both less than 1%, almost unchanged.

We compared the simulation results in this study with the experimental results in the literature by Zhang et al. (2021), as shown in the Figure 4. It can be seen from the figure that although the experimental results are quite different from the simulation results, the change trends of the experimental results and the simulation results are identical. This indicates that the numerical simulation results are credible and the parameters corresponding to the optimal values are correct when using numerical simulation for optimization.

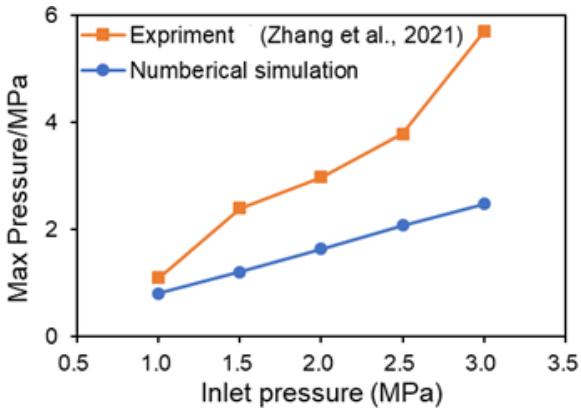

Figure 4. Comparison of maximum pressure value between simulation and experiment.

2.3. Optimization for SEOC's Structure

Based on CFD flow field simulation, a surrogate model is used to optimize the SEOC's multi-objective structure (Dong and Liu, 2021). Figure 5 shows the optimization processes including defining variables, design of test points, model training, global optimization, and error check. The specific implementation steps of the optimization method are as follows.

2.3.1. Defining Variables

In this study, the optimization aims to obtain the optimal structural parameters of SEOC with the preferable cavitation effect. Correspondingly, the optimization object corresponds to the independent variables. The independent variable is defined as the ratio of three structural parameters, namely d_2 / d_1, D / d_2, and L / D. The optimization range of each parameter is 1.5 ~ 3.0 for d_2 / d_1, 4 ~ 9 for D / d_2 and 0.4 ~ 0.7 for L / D.

Generally, vapor volume fraction V_1 in the cavity can directly show the cavitation effect in SEOC. The larger the value of V_1, the more bubbles are generated in the cavity and the better the cavitation effect. Since the bubbles in the cavity are not uniformly distributed, in order to make the result more reasonable, the area-weighted average value is employed to express the vapor volume fraction (V_1) in the cavity. At the same time, in order to facilitate the study of the subsequent part of this topic, it is necessary to study the outlet vapor volume fraction (V_2) of the SEOC. The area weighted average value of vapor volume fraction is shown in Equation (10). Correspondingly, the target

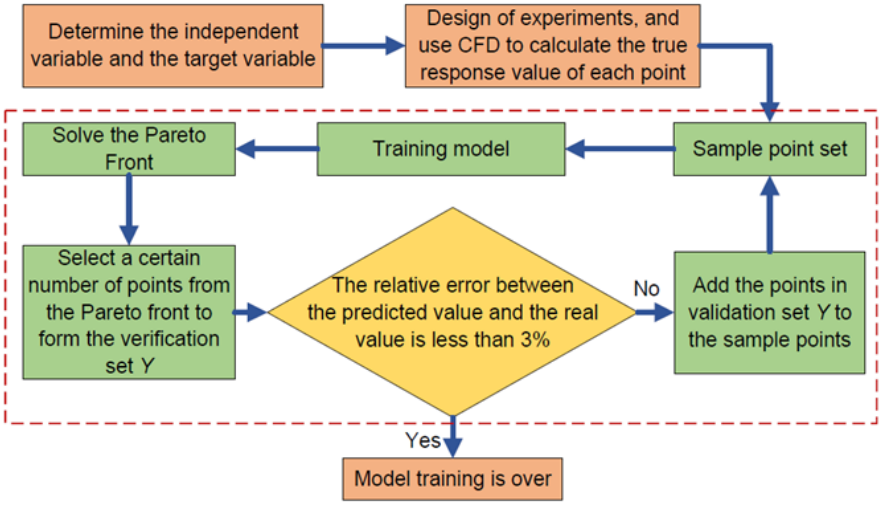

Figure 5. Optimization flow chart.

variables of this study are determined to be V_1 and V_2, as shown in Equations (11) and (12):

$$\bar{v} = \frac{1}{A}\int v dA = \frac{1}{A}\sum_{i=1}^{n} v_i A_i \tag{10}$$

$$V_1 = \bar{v}_{inner} \tag{11}$$

$$V_2 = \bar{v}_{out} \tag{12}$$

where $\bar{v}$ is the area-weighted average of vapor volume fraction, n is the number of grids, A_i is the area of each grid, v_i is the volume fraction of vapor at each grid, $\bar{v}_{inner}$ is the average volume fraction of vapor in the cavity, and $\bar{v}_{out}$ is the average volume fraction of vapor at the outlet.

2.3.2. Design of Experiments

When using the surrogate model, it is very important to design the experimental points. The designed experimental points should cover the entire space within the allowable range of independent variables, and there is an optimal solution in space. At the same time, the experimental points are independent of each other. The commonly used design methods of experimental points include orthogonal experimental design (OET), central composite design, Latin hypercube sampling, optimal Latin hypercube design (OLHD), Box-Behnken and full factor design (FFD) (Aber et al., 2010; Zhang et al., 2011; Sun et al., 2020b).

In this study, OET, OLHD and FFD are selected to design the experimental points, and the advantages and disadvantages of the three methods are compared. Finally, a suitable method for designing experimental points is determined. In this study, leave-one-out cross-validation is used for error analysis, and the correlation coefficient (R^2) and the root mean square error (*RMSE*) are used to characterize the accuracy of the model, and the expressions are as follows:

$$R^2 = 1 - \frac{\sum_{i=1}^{n}(y_i - y_i)^2}{\sum_{i=1}^{n}(y_i - \bar{y})^2} \tag{13}$$

$$RMSE = \sqrt{\frac{\sum_{i=1}^{n}(y_i - y_i)^2}{n}} \tag{14}$$

where n is the number of experimental points, y_i is the real value of the experimental point x_i, y_i is the predicted value of the surrogate model of the experimental point x_i, and $\bar{y}$ is the average of the real response value. The value of R^2 is between 0 and 1, and in this range, the closer the value of R^2 is to 1 and the smaller the *RMSE* value is ($RMSE \geq 0$), the closer the surrogate model is to the real situation, that is, the higher the accuracy.

After calculating the real response value of each experimental point, a batch of sample points are obtained, and R^2 and *RMSE* of different design methods can be obtained by using the sample points to train the surrogate model, as shown in Table 1.

During the experimental processes, each variable has five levels. However, at the same condition, the number of sample points produced by different experimental design methods is different. As shown in Table 1, the best result of model training is full factor design, and the worst is orthogonal experimental design. For OET, because the number of sample points is too small and the sample points contain less model information, the model accuracy is low. At the same time, the experimental point of the orthogonal experimental design is very dependent on the orthogonal table, and it is difficult to obtain a suitable orthogonal experimental design table. FFD can obtain a large amount

of model information because the sample points are full of the whole independent variable space, which makes the surrogate model have high accuracy. However, too many sample points may result in a large amount of calculation, and the calculation of the real response value of the experimental points is very time-consuming. OLHD can artificially control the number of experimental points, and uniform, random and orthogonal sampling in the range of the independent variable, and a large amount of model information can be obtained with fewer points. Therefore, through comprehensively considering calculation amount and model accuracy, OLHD is chosen as the experimental point design method, and the number of experimental points is 50.

Table 1. R^2 and *RMSE* of Different Experimental Point Design Methods

	n	V_1-R^2	V_1-*RMSE*	V_2-R^2	V_2-*RMSE*
OET	25	0.8583	0.1087	0.8466	0.0759
OLHD	50	0.9311	0.0719	0.9348	0.0545
FFD	125	0.9443	0.0636	0.9394	0.0522

2.3.3. Training Surrogate Model

Surrogate model is a mathematical approximation method, which can approximately replace the internal relationship between input and output. Training surrogate model refers to solving the functional relationship between experimental points and experimental or simulation results. This study compares the accuracy of the functional relationships obtained from the Kriging model (KRG), Polynomial response surface model (PRS), Radial basis function model (RBF), Shepard model (SHEP) and a Weighted average surrogate model (WAS) (Goel et al., 2007; Sun et al., 2017; Chen and Wu, 2018).

The WAS model is composed of two models, and the proportion of each model is determined by the model error. Therefore, we first compare the R^2 and *RMSE* of KRG, PRS, RBF and SHEP, and then select two models with better performance to form the WAS model. Finally, the most suitable surrogate model is selected to optimize the SEOC's structure. The experimental point design method adopts OLHD, and the number of experimental points is 50. The accuracy of each model is shown in Table 2. When using a single surrogate model, the accuracy of the functional relationship solved by each model is slightly lower. The two models with better performance are RBF and PRS, which constitute the WAS model. Obviously, the accuracy of the combination of the two models is much higher than the single model. Therefore, the surrogate model used in this optimization scheme is the WAS model composed of PRS and RBF.

2.3.4. Find the Optimal Solution

A genetic algorithm based on multi-objective optimization is used to perform global optimization within the range of independent variables. NSGA-II can reduce the computational complexity and make the individuals of the Pareto front evenly expand to the whole Pareto front. At the same time, it also introduces the elite strategy to effectively prevent the loss of the best individual and improve the accuracy of the optimization results (Na et al., 2017; Mansour et al., 2020; Wang et al., 2020a). In this study, the Pareto optimal solutions with the best cavitation effect are obtained by using NSGA-II optimization algorithm, taking d_2 / d_1, D / d_2 and L / D as design variable and V_1 and V_2 as optimization targets.

Table 2. R^2 and *RMSE* of KRG, SHEP, RBF, PRS and WAS

	V_1-R^2	V_1-*RMSE*	V_2-R^2	V_2-*RMSE*
SHEP	0.3957	0.2844	0.4346	0.2293
KRG	0.4158	0.2093	0.5274	0.1466
RBF	0.5282	0.1881	0.5502	0.1430
PRS	0.6353	0.1654	0.6436	0.1273
WAS	0.9311	0.0719	0.9348	0.0545

2.3.5. Error Check (adding point strategy)

Since both V_1 and V_2 are small values between 0 and 1, after obtaining the Pareto optimal solutions, it is necessary to perform error analysis on the points in the solution set to ensure that the optimal solution with the higher accuracy can be obtained. In this study, a small number of design points were randomly selected for verification. Five verification points are uniformly selected from the Pareto front solutions, as shown in Figure 6(a), to form the verification set $Y = \{Y_1, Y_2, Y_3, Y_4, Y_5\}$. Then, the structural parameters corresponding to Y_i are found, and the real response values at each point are calculated through CFD. Finally, the relative error at the corresponding point is calculated as follow:

$$Re_i = \frac{|Y_i - y_i|}{y_i} \times 100\%, \ (i = 1,2,3,4,5) \tag{15}$$

where Y_i is the predicted value of the surrogate model, and y_i is the real value at that point. If the relative error Re_i is less than 3%, the value of Pareto optimal solutions is considered to be accurate. On the contrary, it shows that the value error of Pareto optimal solutions is large, and the accuracy of surrogate model needs to be further improved. This requires expanding the number of samples to reduce errors. This study adopts the method of adding points based on prediction to expand the sample size. It is a method of adding points at the minimum approximate value of the training point space to make the optimization result converge to the optimal value, that is, adding the points in the set Y to the sample points. Then, the process (as shown in Figure 5) is executed again until the error condition is satisfied, and the iteration is terminated.

In this study, the convergence condition is satisfied after 4 iterations, so that the relative error of the model is less than 3%, and the number of samples is increased from 50 to 70. In each step of iteration, the fitting error of WAS is always smaller than that of other surrogate models. The R^2 and RMSE of the surrogate model at the initial and after convergence are presented in Table 3, and the relative error of each point in validation set Y is listed in Table 4.

As can be seen from Tables 3 and 4, when only the initial

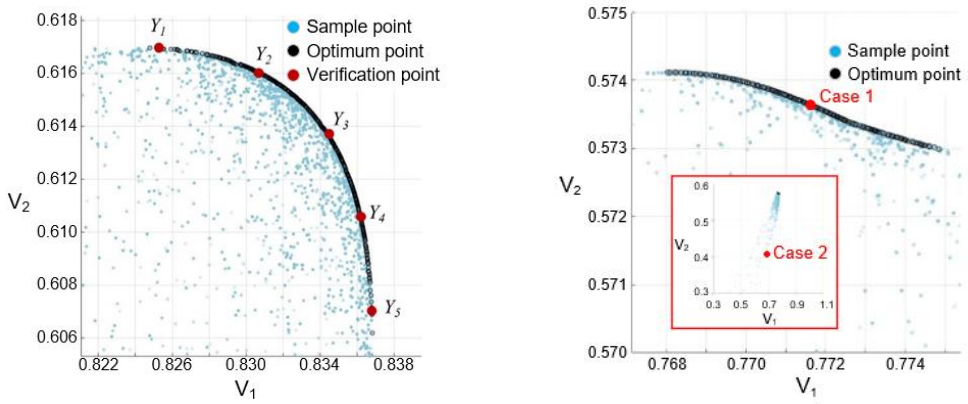

(a) Distribution of sample points

(b) Pareto optimal solutions

Figure 6. Pareto front solutions (the black point is the Pareto optimal solutions, and the red point is the verification point selected from the Pareto optimal solutions).

sample points are used, the surrogate model fits the two target variables well. However, in the local position (Pareto optimal solutions), the fitting effect of V_1 is better, and the fitting effect of V_2 is slightly worse. After adding points locally to iterative convergence, the R^2 and *RMSE* of the surrogate model are improved or decreased, indicating that the accuracy of the model has been further improved. Meanwhile, it can be seen from the relative error that the fitting effect of V_1 and V_2 is improved at the local position (Pareto optimal solutions). This is because the newly added sample points are taken from the Pareto optimal solutions, namely, the added sample points are very close to the expected Pareto front, which greatly improves the accuracy of the sample points and makes the model converge quickly. Therefore, the local adding point strategy of adding the points of the verification set to the sample points can ensure the accuracy of the obtained Pareto optimal solutions, without adding too many sample points and not generating too much computation.

Through the above steps, we can finally get a more accurate Pareto front solutions as shown in Figure 6(b). Pareto front solutions is a set in which the points are all the optimal solution.

3. Result and Discussion

3.1. Formation Process of Cavitation Airbag

Figure 7 shows the vapor distribution in the SEOC at different times. Cavitation is initially generated near the upstream, and when it develops downstream, vortices and cavitation bubbles begin to accumulate near the collision wall due to the blocking of the collision wall, as shown in Figure 7(a). Subsequently, the vortex gradually becomes larger, and the negative pressure area in the cavity expands, resulting in many cavitation bubbles. The cavitation bubbles combine with each other to form larger vapor bubbles, and gradually move to the center of the cavity, as shown in Figure 7(b). Finally, the vortex is further enlarged and moved to the center of the cavity to form a large negative pressure area, and numerous cavitation bubbles form cavitation airbag in the cavity. At the same time, part of the cavitation vortex moves downstream of the nozzle with the jet, forming the vapor distribution diagram as shown in Figure 7(c). The formation process of the cavitation airbag proves that the SEOC can generate effective disturbance feedback, so that the vortex can be formed in the cavity, and the vortex can be magnified in a very short time to form a negative pressure region, thereby causing cavitation. At the same time, in this process, the cavitation region will also become larger with the increase of the vortex, and the cavitation bubbles in the cavity will gradually increase.

Table 3. R^2 and *RMSE* of the Surrogate Model

	n	V_1-R^2	V_1-*RMSE*	V_2-R^2	V_2-*RMSE*
Initially	50	0.9311	0.0719	0.9348	0.0545
After convergence	70	0.9424	0.0621	0.9497	0.0469
Improvement	—	1.21%	13.59%	1.60%	13.93%

Table 4. Relative Error of Each Point in The Verification Set

		Y_1	Y_2	Y_3	Y_4	Y_5
Initial relative error (n = 50)	V_1	1.97%	3.03%	3.55%	0.93%	1.75%
	V_2	7.92%	5.65%	7.89%	7.03%	9.23%
Relative error after convergence (n = 70)	V_1	1.60%	1.54%	1.19%	1.13%	2.05%
	V_2	0.18%	0.37%	0.27%	1.20%	1.73%

3.2. Global Sensitivity Analysis

In order to intuitively explain the changes of the target variables V_1 and V_2 to the structure parameters d_2 / d_1, D / d_2, and L / D, the response surface analysis is conducted, as shown in Figure 8. Figure 8(a), (b), and (c) show the influence of various parameters on the vapor volume fraction V_1 in the cavity. As can be seen from the figures, V_1 increases and then decreases with increasing D / d_2, decreases with increasing L / D, and increases with increasing d_2 / d_1. Figure 8(d), (e) and (f) show the influence of various parameters on the outlet vapor volume fraction V_2. As can be seen from the figures, V_2 decreases with the

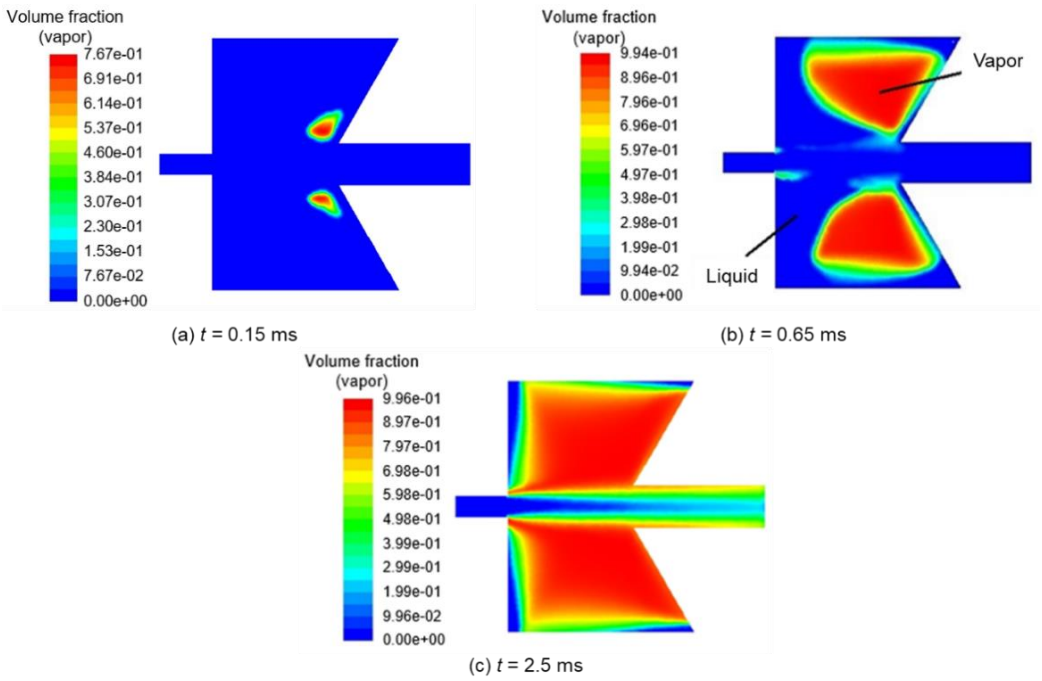

Figure 7. Formation process of the cavitation airbag in the SEOC. (a), (b), and (c) are the vapor volume fractions of 0.15, 0.65, and 2.5 ms, respectively.

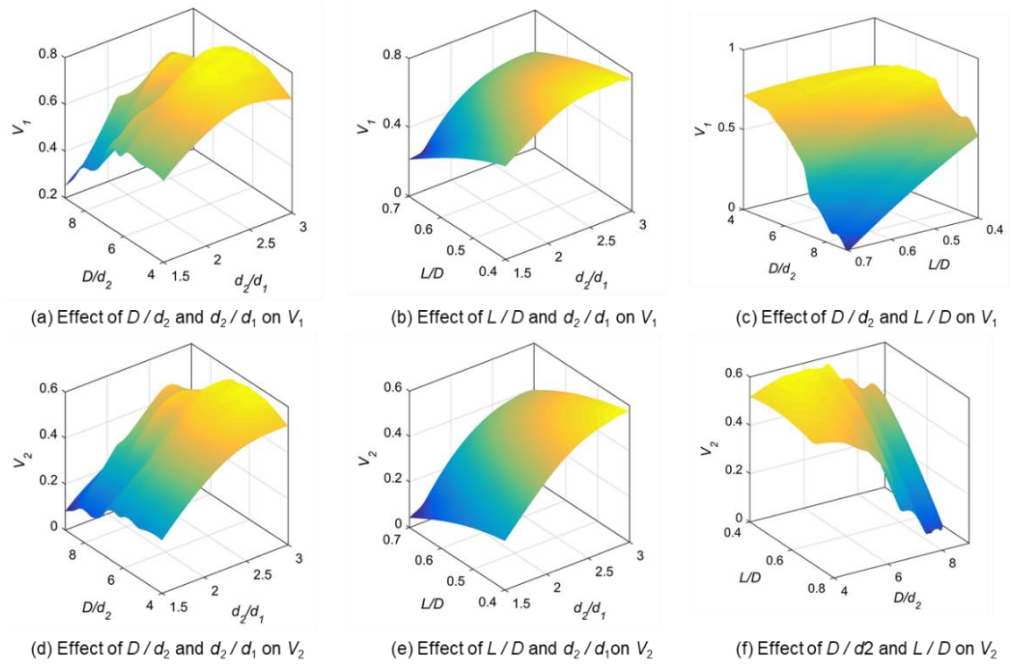

Figure 8. Influence of each parameter on the target variable.

increase of D / d_2 and L / D, and increases with the increase of d_2 / d_1. Through the response surface, the influence of each parameter on the target variable can be seen intuitively, but the interaction between the parameters cannot be explored, and the global sensitivity analysis of each parameter is carried out.

In this study, sobol sensitivity analysis (SSA) method, based on variance decomposition, is used for global sensitivity analysis to explore the degree of effect of each variable on the target variable (Ren *et al*., 2010). Compared with other sensitivity approaches, SSA can analyze the sensitivity of the first, second and higher order of parameters, and can also distinguish the sensitivity of parameter independence and interaction. SSA es-

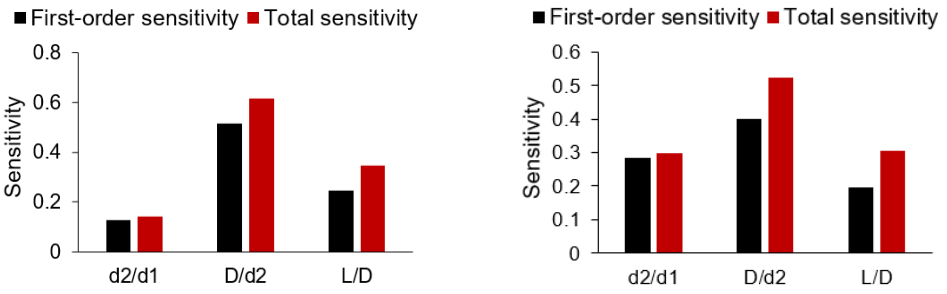

(a) the first-order sensitivity and total sensitivity of each parameter to V_1

(b) the first-order sensitivity and total sensitivity of each parameter to V_2

Figure 9. First-order sensitivity and total sensitivity.

timates the contribution of each parameter and its interactions based on the variance. The contribution of input parameters to the model output and the interaction between them can be estimated using Equation (16). The first-order sensitivity S_i and total sensitivity S_{Ti} are expressed by Equations (17) and (18), respectively (Kumar *et al*., 2020; Abbiati *et al*., 2021):

$$D(y) = \sum_i D_i + \sum_{i<j} D_{ij} + \sum_{i<j<k} D_{ijk} + D_{12\ldots p} \tag{16}$$

$$S_i = \frac{D_i}{D} \tag{17}$$

$$S_{Ti} = 1 - \frac{D_{\sim i}}{D} \tag{18}$$

where $D(y)$ is the total variance of the output of each parameter, D_i is the variance generated by x_i, D_{ij} is the variance generated by the interaction of x_i and x_j, D_{ijk} is the variance generated by the interaction of x_i, x_j, and x_k, $D_{12\ldots p}$ is the variance generated by the interaction of x_1, …, x_p, and $D_{\sim i}$ is the variance of all parameters except parameter x_i.

The first-order sensitivity represents the effect of the change of a single parameter on the target variable, and the total sensitivity also reflects the effect of interaction with other parameters. The difference between S_i and S_{Ti} represents the strength of the interaction effect between the parameters. The greater the difference is, the stronger the interaction between parameters is. Therefore, when the difference is small, the effect of the interaction of the parameters is small and can be ignored (Shu *et al*., 2018). When V_1 and V_2 are the target variables, the S_i and S_{Ti} of the optimized parameters d_2 / d_1, D / d_2 and L / D of the SEOC are shown in Figure 9.

According to the first-order sensitivity, D / d_2 has the highest effect on the target variable V_1, followed by L / D, and d_2 / d_1 has the lowest effect; while D / d_2 has the highest effect on the target variable V_2, followed by d_2 / d_1, and L / D has the lowest effect. To sum up, D / d_2 has the highest degree of effect on the target variable, and then special attention needs to be paid to this parameter when optimizing the structure of the SEOC. However, L / D and d_2 / d_1 have different effects on V_1 and V_2. This may be due to the fact that L / D affects the size of the cavity, which affects the vapor volume fraction in the cavity, while d_2 / d_1 affects the outlet diameter, which affects the vapor volume fraction at the outlet, resulting in the difference of the effect of these two parameters on V_1 and V_2. It can be seen from Figure 9 that the difference between the S_i and S_{Ti} of d_2 / d_1 is small, while the difference between the S_i and S_{Ti} of D / d_2 and L / D is large. This shows that d_2 / d_1 does not interact with other parameters, but the interaction between D / d_2 and L / D has an effect on the target variables. Therefore, in the optimization process, we should not only focus on the effect of each parameter on the cavitation effect of the self-excited oscillating cavity, but also consider the interaction between the parameters, and then reasonably to select the combination of the parameters.

3.3. Comparison before and after Structural Optimization

In order to verify the superiority of each point in the Pareto front solutions, the structure in the solution set is simulated and compared with the SEOC structure existed in our laboratory. The structural parameters of the self-oscillation cavity selected from the Pareto optimal solution (Case 1) and the structural parameters of the SEOC (Case 2) existed in our laboratory and the results of the numerical simulation using CFD simulation are shown in Table 5. The positions of Case 1 and Case 2 are shown in Figure 6(b). The structural parameters of Case 1 are taken from the middle value of the Pareto front solutions and Case 2 is the original device parameters in our laboratory. The vapor phase distribution in the cavity is shown in Figure 10. The formula of improvement degree is defined as follows:

$$\text{Improvement degree} = \frac{V_{Case1} - V_{Case2}}{V_{Case2}} \ 100\% \tag{19}$$

where V_{Case1} refers to V_1 in Case1 and V_{Case2} refers to V_2 in Case2.

From the simulation results of the two structures, it can be seen that the calculation results of the Case 1 structure are greatly improved compared with the Case 2, in which V_1 and V_2 are improved by 13.46 and 38.01% respectively. This shows that the cavitation effect of the SEOC obtained by this optimization scheme is better than that of the existing SEOC existed in our

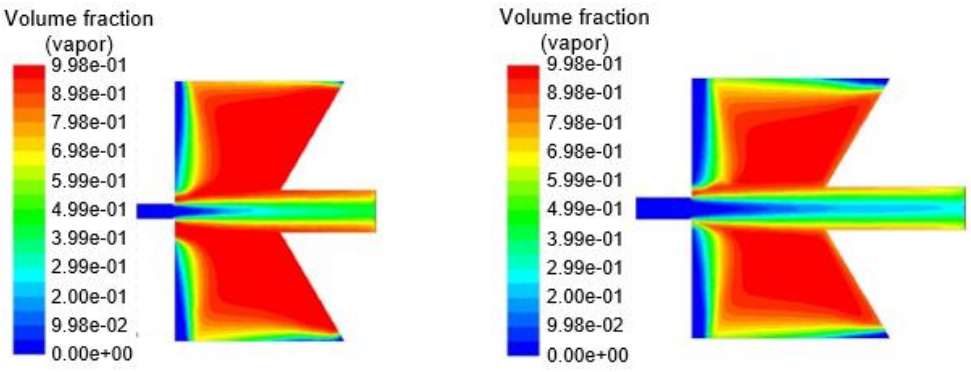

(a) Case 1 (b) Case 2

Figure 10. Vapor volume fraction distribution diagram of (a) Case 1 and (b) Case 2.

laboratory, which proves the superiority of each point in the Pareto optimal solutions. As can be seen from Figure 10, the proportion of vapor in the SEOC of Case 1 is relatively high, and the cavitation bubble almost fills the whole cavity. While in Case 2, there is a higher proportion of vapor only near the center of the cavity, a lower proportion of vapor and less cavitation bubbles at the edge of the cavity. This indicates that the space utilization rate of the SEOC of Case 1 is higher, and it also shows that the structure can generate more cavitation bubbles in the cavity, which makes the SEOC generate better cavitation effects. In addition, there are more bubbles in the exit jet of the SEOC of Case 1, which is beneficial to the study of SEOC cavitation in the future.

Table 5. Structural Parameters and CFD Simulation Results

	d_2/d_1	D/d_2	L/D	V_1	V_2
Case 1	2.88	6.09	0.4	0.7770	0.5631
Case 2	2.0	6.0	0.5	0.6848	0.4080
Improvement				13.46%	38.01%

3.4. Study on Methylene Blue Degradation

The numerical simulation results show that the vapor volume fraction of the optimized SEOC (Case 1) is significantly higher than that of the original SEOC (Case 2). This proves that the cavitation intensity of the optimized SEOC is improved, so that the water treatment capacity of the SEOC will be improved. In order to verify the water treatment effect of the optimized SEOC, methylene blue (MB) degradation experiments were carried out on the optimized SEOC and the original SEOC.

In the process of HC, the degradation of MB may be due to the formation of hydroxyl radicals, so it is directly affected by the cavitation intensity. MB is relatively stable in air, its solution is non-volatile and can react with hydroxyl radicals quickly, so it is very suitable as a substrate for HC degradation experiment. The experimental system setup is shown in Figure 11. There are two lines in the system, the main line and the bypass line. The main line mainly includes tank, pump, control valve, pressure gauge and HC generating device (SEOC). During the experiment process, one side of the pump is connected with the water tank, and the other side is connected with the control valve to make the waste water enter the nozzle, and then the cavitation occurs in the nozzle, and finally the waste water is discharged back to the water tank from the outlet. The pressure gauge monitors the inlet pressure of the nozzle, and the bypass line regulates the pressure and protects the circuit.

During the experiment, the absorbance of MB solution was measured by the ultraviolet spectrophotometer (Figure 12(a), UV759CRT, wavelength range 190 ~ 1100 nm, MB solution has the best absorbance value at the wavelength of 664 nm). As shown in Figure 12(b), the standard curve of methylene blue solution concentration is obtained by configuring different concentrations of MB solution to calibrate the relationship between absorbance (A) and MB solution concentration (C_{MB}). The concentration of MB solution can be converted from the absorbance of the solution.

During the experiment, the inlet pressure of Case 1 and Case 2 is 1 MPa, the outlet pressure is atmospheric pressure, the initial concentration of MB solution is 15 μmol/L, the solution volume is 5 L, the solution temperature is 25 ℃, the treatment time is 120 min, and the sampling interval is 15 min. To ensure that the experimental conditions were in the cavitation state, the cavitation number was calculated as shown in Equation (20):

$$\sigma = \frac{p_2 - p_v}{\frac{1}{2}\rho v_0^2} \tag{20}$$

where p_2 is the downstream pressure, v_0 is the fluid velocity, and p_v and ρ are the vapor pressure and density of the liquid, respectively. According to the formula, the cavitation number in the self-excited oscillation cavity under the experimental conditions in this study is 0.12. Theoretically, cavitation can occur if the cavitation number is less than 1, and stable cavitation is inevitably produced if the cavitation number is less than 0.5. Therefore, the experimental conditions in this study are in a state of cavitation. The degree of degradation and degradation rate of MB solution under different conditions are shown in Figure 13.

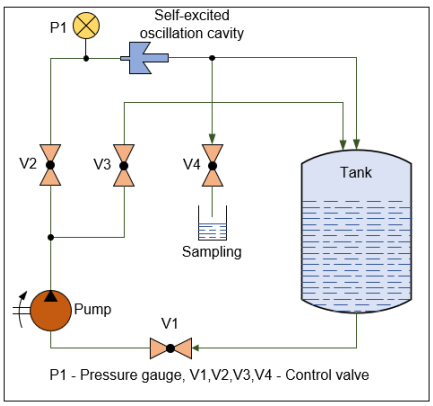

(a) Schematic diagram of water treatment unit

(b) Experimental system setup diagram

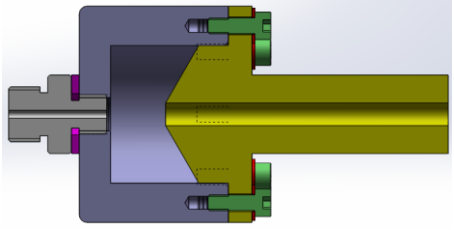

(c) Three-dimensional cross-sectional view

(d) SEOC device

Figure 11. Experimental equipment and system schematic diagram.

(a) Sample and absorbance measuring equipment

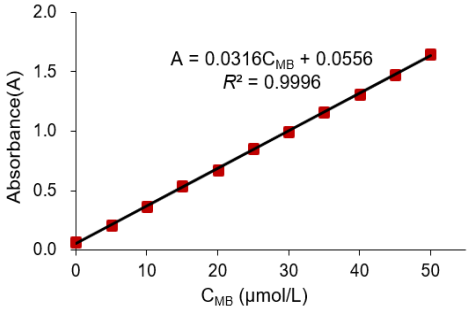

(b) Concentration standard curve

Figure 12. Concentration standard curve of methylene blue solution.

It can be seen from Figure 13(a) that after 120 min of treatment time, the degree of degradation of MB in Case 1 and Case 2 is 16.14 and 10.12%, respectively, which is increased by 59.5%. This means that the removal efficiency of MB in the optimized SEOC is obviously better than that in the original SEOC. Figure 13(b) shows the relationship between the first-order kinetics $\ln(C_0 / C)$ and time (the first-order model fits well, C is the concentration of MB solution and C_0 is the initial concentration of MB solution). It can be seen from Figure 13(b) that the MB degradation rate of Case 1 (1.4×10^{-3} min^{-1}) is also significantly higher than that of Case 2 (0.9×10^{-3} min^{-1}).

Similar results have been reported by some scholars. Li *et al*. (2017) carried out MB degradation experiment with the optimized orifice plate, and reported that the removal rate of HC alone was less than 3%. Çalışkan *et al*. (2017) studied the degradation effect of HC on RR180 in a pilot reactor, and reported that the removal efficiency of RR180 was only 4.6% when HC was used alone. Wang et al. (2020b) also presented similar experimental results in the process of HC degradation of textile wastewater, and the degradation degree of HC alone was only 8.16%. It is indicated that the degradation capacity of organic matter by HC is limited, and the removal of MB by HC alone is not significant. In summary, the comparative experiment shows that the optimization method of this study can obtain the preferable SEOC structure parameters, which proves the effectiveness of the optimization method.

3.5. Future Research Work

In this study, OLHD, surrogate model, NSGA-II and uniform point addition strategy are used in the optimization pro-

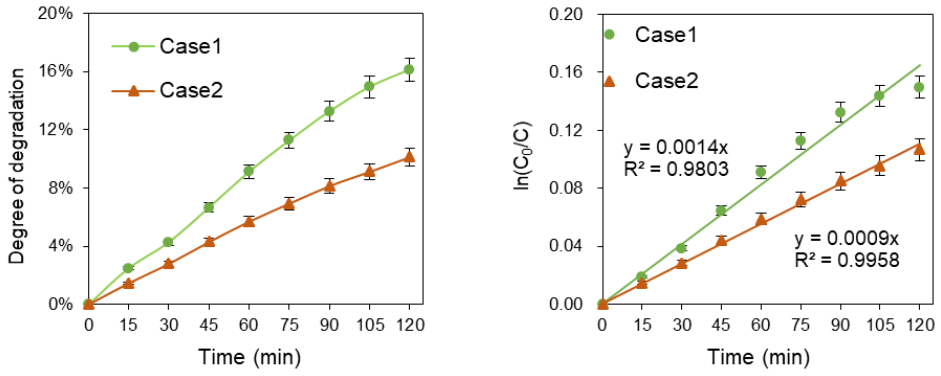

(a) Degree of degradation

(b) First-order kinetic fitting

Figure 13. (a) Degree of degradation and (b) first-order kinetic fitting.

cess. The use of these methods has achieved good optimization results, but this is not the most perfect result. For example, experimental design method and addition strategy used need to be further explored. Although OLHD has achieved good results, the amount of calculation generated by the sample points is still relatively large, so it is necessary to further explore the experimental design method which can reduce the amount of calculation while ensuring the same results. As for the addition strategy, this study only uses the simplest method, the addition strategy also needs to be improved. For instance, the expected improvement (EI) adding point criterion has the ability to develop the local optimal region and explore the potential optimal region, which can increase the iterative convergence speed in the optimization process and improve the utilization efficiency of simulation or experimental resources (Liu *et al*., 2018; Zhang *et al*., 2018). Finally, although the experimental study of MB wastewater degradation was carried out, it was verified that the degree of degradation of the SEOC was significantly improved after optimization. However, the degradation effect of HC is not obvious when it is used alone, so it is necessary to further explore the methods to improve the degradation effect of HC technology. Furthermore, the optimization method proposed in this study is suitable not only for the optimization of SEOC, but also for the other similar flow field optimization problems.

4. Conclusions

This study aims to develop an integrated method for optimizing the structure of SEOC, which incorporates techniques of CFD simulation, surrogate model, and NSGA-II within a general framework. In this study, the vapor volume fraction in the cavity and the vapor volume fraction at the outlet are taken as the optimization objectives, aiming at the problems of inaccurate optimal structure and large amount of calculation in the optimization design of SEOC, an optimization design method of SEOC structure for AOPs based on surrogate model and CFD simulation is proposed to obtain the preferable cavitation effect. The following conclusions were drawn from this study.

(1) The combination of techniques of CFD simulation, surrogate model and NSGA-II is applied to the structural optimization design of SEOC to improve the cavitation effect of SEOC, so as to improve the yield of hydroxyl radicals in the cavitation process, and finally improve the degradation degree of wastewater.

(2) An optimization method of SEOC structure based on surrogate model is proposed. A set of SEOC structure parameters obtained by this optimization method are $d_2 / d_1 = 2.88$, $D / d_2 = 6.09$, and $L / D = 0.4$. Compared with the SEOC existed in our laboratory, the vapor volume fraction in the cavity and the vapor volume fraction at the outlet is increased by 13.46% and 38.01% respectively, thus enhancing the cavitation intensity and improving the degradation efficiency.

(3) The global sensitivity analysis is carried out by using Sobol sensitivity analysis method to explore the effect of each parameter on the target variable. The analysis shows that the effect degree of the target variable V_1 from high to low is D / d_2, L / D and d_2 / d_1; the effect degree of the target variable V_2 from high to low is D / d_2, d_2 / d_1 and L / D; and the interaction between the parameters D / d_2 and L / D will affect the cavitation effect of the SEOC.

(4) The degradation experiment of MB is carried out on the SEOC before and after the optimization, and the degree of degradation was 10.12 and 16.14%, respectively, and the degradation capacity increases by 59.5%. This shows that the degree of degradation of MB in the self-excited oscillating cavity after optimization is significantly improved, which verifies that the optimization method in this study is effective.

This study will not only play a significantly guiding role on the optimization design of SEOC for AOPs to obtain the preferable cavitation effect, but also provide support for the optimization of a class of hydrodynamic structure problems.

Acknowledgments. The authors would like to thank the National Natural Science Foundation of China (Grant Nos. 51975010, 51905011, 52075007, and 52005013), General Program of Science and Technology Development Project of Beijing Municipal Education Commission (Grant Nos. KM201810005014, KM201910005033 and KM202110005031) and Beijing Postdoctoral Research Foundation (Grant No. 2020-ZZ-033). The authors are very grateful to the editors and the anonymous reviewers for their insightful comments and suggestions.

References

Abbiati, G., Marelli, S., Tsokanas, N., Sudret, B. and Stojadinović, B. (2021). A global sensitivity analysis framework for hybrid simulation. *Mech. Syst. Signal Pr.*, 146, 106997. https://doi.org/10.1016/j.ymssp.2020.106997

Aber, S., Salari, D. and Parsa, M.R. (2010). Employing the Taguchi method to obtain the optimum conditions of coagulation flocculation process in tannery wastewater treatment. *Chen. Eng. J.*, 162(1), 127-134. https://doi.org/10.1016/j.c ej.2010.05.012

Asztalos, J.R. and Kim, Y. (2017). Lab-scale experiment and model study on enhanced digestion of wastewater sludge using Bioelectrochemical systems. *J. Environ. Inform.*, 29(2), 98-109. https://doi.org/10.3808/jei.201500308

Bhat, A.P. and Gogate, P.R. (2020). Degradation of nitrogen containing hazardous compounds using advanced oxidation processes: A review on aliphatic and aromatic amines, dyes, and pesticides. *J. Hazard Mater.*, 403, 123657. https://doi.org/10.1016/j.jhazmat.2020.123657

Çalışkan, Y., Yatmaz, H.C. and Bektaş, N. (2017). Photocatalytic oxidation of high concentrated dye solutions enhanced by hydrodynamic cavitation in a pilot reactor. *Process Saf. Environ.*, 111, 428-438. https://doi.org/10.1016/j.ps ep.2017.08.003

Chakinala, A.G., Gogate, P.R., Burgess, A.E. and Bremner, D.H. (2009). Industrial wastewater treatment using hydrodynamic cavitation and heterogeneous advanced Fenton processing. *Chen. Eng. J.*, 152(2), 498-502. https://doi.org/10.1016/j.cej.2009.05.018

Chen, J. and Wu, G.Q. (2018). Kriging-assisted design optimization of the impeller geometry for an automotive torque converter. *Struct. Multidiscip. O.*, 57(6), 2503-2514. https://doi.org/10.1007/s00158-017-1857-3

Doltade, S.B., Dastane, G.G., Jadhav, N.L., Pandit, A.B. Pinjari, D.V., Somkuwar, N. and Paswan, R. (2019). Hydrodynamic cavitation as an imperative technology for the treatment of petroleum refinery effluent. *J. Water Process Eng.*, 29, 100768. https://doi.org/10.1016/j.jwpe.2019.02.008

Dong, X. and Liu, X.M. (2021). Multi-objective optimization of heat transfer in microchannel for non-Newtonian fluid. *Chen. Eng. J.*, 412, 128594. https://doi.org/10.1016/j.cej.2021.128594

Fang, Z.L., Zeng, F.D., Xiong, T., Wei, W., Jiang, P., Wu, Q., Wang, Y.S. and Fei, Y.X. (2020). Large eddy simulation of self-excited oscillation inside Helmholtz oscillator. *Int. J. Multiphas. Flow*, 126, 103253. https://doi.org/10.1016/j.ijmult iphaseflow.2020.103253

Franke, M., Braeutigam, P., Wu, Z.L., Ren, Y.Z. and Ondruschka, B. (2011). Enhancement of chloroform degradation by the combination of hydrodynamic and acoustic cavitation. *Ultrason Sonochem.*, 18(4), 888-894. https://doi.org/10.1016/ j.ultsonch.2010.11.011

Geveci, M., Oshkai, P., Rockwell, D., Lin, J.C. and Pollack, M. (2003). Imaging of the self-excited oscillation of flow past a cavity during generation of a flow tone. *J. Fluid. Struct.*, 18(6), 665-694. https://doi.org/10.1016/j.jfluidstructs.2003.0 7.017

Goel, T., Haftka, R.T., Shyy, W. and Queipo, N.V. (2007). Ensemble of surrogates. *Struct. Multidiscip. O.*, 33(3), 199-216. https://doi.org/10.1007/s00158-006-0051-9

Gogate, P.R. (2020). Cavitation: an auxiliary technique in wastewater treatment schemes. *Adv. Environ. Res.*, 6, 335-358. https://doi.org/10.1016/S1093-0191(01)00067-3

Huang, B., Young, Y.L., Wang, G.Y. and Shyy, W. (2013). Combined Experimental and Computational Investigation of Unsteady Structure of Sheet/Cloud Cavitation. *J. Fluid. Eng.*, 135(7), 071301. https://doi.org/10.1115/1.4023650

Jin, L. and Mi, Z.N. (2016). Structure Optimization of Deep Sea Self-excited Oscillation Nozzle. *Fluid Power Transmission and Control*, 02, 24-26. https://doi.org/10.3969/j.issn.1672-8904.2016.02.006. (in Chinese)

Kumar, D., Singh, A., Kumar, P., Jha, R.K., Sahoo, S.K. and Jha, V. (2020). Sobol sensitivity analysis for risk assessment of uranium in groundwater. *Environ. Geochem. Hlth.*, 42(6), 1789-1801. https://doi.org/10.1007/s10653-020-00522-5

Li, D., Kang, Y., Ding, X.L., Wang, X.C. and Fang, Z.L. (2016). Effects of area discontinuity at nozzle inlet on the characteristics of highspeed self-excited oscillation pulsed waterjets. *Exp. Therm. Fluid Sci.*, 79, 254-265. https://doi.org/10.1016/j.expthermflusci.2016.07.013

Li, G.S., Yi, L.D., Wang, J. and Song, Y.T. (2020). Hydrodynamic cavitation degradation of Rhodamine B assisted by Fe^{3+}-doped-TiO_2: Mechanisms, geometric and operation parameters. *Ultrason Sonochem.*, 60, 104806. https://doi.org/10.1016/j.ultsonch.2019.104806

Li, X.L., Huang, B., Chen, T.R., Liu, Y., Qiu, S.C. and Zhao. J. (2017). Combined experimental and computational investigation of the cavitating flow in an orifice plate with special emphasis on surrogate based optimization method. *J. Mech. Sci. Technol.*, 31(1), 269-279. https://doi.org/10.1007/s12206-016-1229-8

Liu, Y.X., Chen, S.S., Wang, F.G. and Xiong, F.F. (2018). Sequential optimization using multi-level cokriging and extended expected improvement criterion. *Struct. Multidiscip. O.*, 58(3), 1155-1173. https://doi.org/10.1007/s00158-018-1959-6

Mansour, M., Zahringer, K., Nigam, K.D.P., Thevenin, D. and Janiga, G. (2020). Multi-objective optimization of liquid-liquid mixing in helical pipes using Genetic Algorithms coupled with Computational Fluid Dynamics. *Chen. Eng. J.*, 391, 123570. https://doi.org/10.1016/j.cej.2019.123570

Mishra, K.P. and Gogate, P.R. (2010). Intensification of degradation of Rhodamine B using hydrodynamic cavitation in the presence of additives. *Sep. Purif. Technol.*, 75(3), 385-391. https://doi.org/10.1016/j.seppur.2010.09.008

Na, J., Kshetrimayum, K.S., Lee, U. and Han, C, (2017). Multi-objective optimization of microchannel reactor for Fischer-Tropsch synthesis using computational fluid dynamics and genetic algorithm. *Chen. Eng. J.*, 313, 1521-1534. https://doi.org/10.1016/j.cej.2016.11.040

Patil, P.N., Bote, S.D. and Gogate, P.R. (2014). Degradation of imidacloprid using combined advanced oxidation processes based on hydrodynamic cavitation. *Ultrason Sonochem.*, 21(5), 1770-1777. https://doi.org/10.1016/j.ultsonch.2014.02.024

Rajoriya, S., Bargole, S. and Saharan, V.K. (2017). Degradation of a cationic dye (Rhodamine 6G) using hydrodynamic cavitation coupled with other oxidative agents: Reaction mechanism and pathway. *Ultrason Sonochem.*, 34, 183-194. https://doi.org/10.1016/j.ultsonch.2016.05.028

Ren, Q.W., Chen, Y.B., Zhou, H.L. and Xu, H.J. (2010). Global sensitivity analysis of TOPMODEL parameters based on Sobol method. *Yangtze River*, 41(19), 91-94. https://doi.org/10.16232/j.cnki.1001-4179.2010.19.028 (in Chinese)

Shu, R.Z., Wei, J., Qin, D.T., Lim, T.C. and Zhang, A.Q. (2018). Global sensitivity analysis and dynamic optimization of multi-motor driv-ing transmission system. *Struct. Multidiscip. O.*, 58(2), 797-816. https://doi.org/10.1007/s00158-018-1909-3v

Sun, G.Y., Zhang, H.L., Fang, J.G., Li, G.Y. and Li, Q. (2017). Multi-objective and multi-case reliability-based design optimization for tailor rolled blank (TRB) structures. *Struct. Multidiscip. O.*, 55(5), 1899-1916. https://doi.org/10.1007/s00158-016-1592-1

Sun, T.Z., Wei, Y.J. and Wang, C. (2015). Prediction of cryogenic cavitation around hydrofoil by an extensional Schnerr-Sauer cavitation model. *J. Phy. Confer. Ser.*, 656, 012180. https://doi.org/10.1088/1742-6596/656/1/012180

Sun, X., Liu, J.T., Ji, L., Wang, G.C., Zhao, S., Yoon, J.Y. and Chen, S.Y. (2020a). A review on hydrodynamic cavitation disinfection: The current state of knowledge. *Sci. Total Environ.*, 737, 139606. https://doi.org/10.1016/j.scitotenv.202 0.139606

Sun, Y.B., Meng, X.Y., Long, T. and Wu, Y.F. (2020b). A fast optimal

Latin hypercube design method using an improved translational propagation algorithm. *Eng. Optimiz.*, 52(7), 1244-1260. https://doi.org/10.1080/0305215X.2019.1642881

Thanekar, P., Gogate, P.R., Znak, Z., Sukhatskiy, Y. and Mnykh, R. (2021). Degradation of benzene present in wastewater using hydrodynamic cavitation in combination with air. *Ultrason Sonochem.*, 70, 105296. https://doi.org/10.1016/j.ultsonch.2020.1 05296

Thanekar, P., Panda, M. and Gogate, P.R. (2018). Degradation of carbamazepine using hydrodynamic cavitation combined with advanced oxidation processes. *Ultrason Sonochem.*, 40, 567-576. https:// doi.org/10.1016/j.ultsonch.2017.08.001

Wang, J.H., Chen, H.L., Yuan, R.F., Wang, F., Ma, F.S. and Zhou,B.H. (2020b). Intensified degradation of textile wastewater using a novel treatment of hydrodynamic cavitation with the combination of ozone. *J. Environ. Chem. Eng.*, 8(4), 103959. https://doi.org/10.1016/j.jece.2020.103959

Wang, X.M. (2005). *Influence factors numerical simulation study of the self-excited oscillation pulsed jet device and nozzle structure optimized design*. Ph.D. Dissertation, Zhejiang University, Hangzhou, China. (in Chinese)

Wang, Y., Li, C.S., Jin, X., Xiang, Y.G. and Li, X.G. (2020a). Multi-objective optimization of rolling schedule for tandem cold strip rolling based on NSGA-II. *J. Manuf. Process.*, 60, 257-267. https://doi.org/10.1016/j.jmapro.20 20.10.061

Wang, Z.H., Chen, S. and Deng, X.G. (2017). Research on modified cavitation model for self-excited oscillation pulsed jet nozzle. *2017 International Conference on Mechanical, System and Control Engineering (ICMSC)*, pp 90-95. https://doi.org/10.1109/ICMSC.2017.7959449

Wang, Z.H., Sun, X. and Chen, S. (2019). Multi-objective parameters optimization design of self-excited oscillation pulsed atomizing nozzle. *J. Braz. Soc. Mech. Sci.*, 41(11), 510. https://doi.org/10.1007/s40430-019-1975-5

Xiang, L.H., Wei, X.S. and Chen, S.Y. (2020). Experimental study on the frequency characteristics of self-excited pulsed cavitation jet. *Eur. J. Mech. B-Fluid.*, 83, 66-72. https://doi.org/10.1016/j.eurome chflu.2020.04.006

Yi, C.H., Lu, Q.Q., Wang, Y., Wang, Y.X. and Yang, B.L. (2018). Degradation of organic wastewater by hydrodynamic cavitation combined with acoustic cavitation. *Ultrason Sonochem.*, 43, 156-165. https://doi.org/10.1016/j.ultsonch.2018.01.0 13

Yi, L.D., Li, B.Q., Sun, Y.N., Li, S., Qi, Q.Q., Qin, J., Sun, H.S.,Wang, X.R., Wang, J. and Fang, D.W. (2021). Degradation of norfloxacin in aqueous solution using hydrodynamic cavitation: Optimization of geometric and operation parameters and investigations on mechanism. *Sep. Purif. Technol.*, 259, 118166. https://doi.org/10.1016/j.seppur.2020.118166

Zhang, P.P., Breitkopf, P., Knopf-Lenoir, C. and Zhang, W.H. (2011). Diffuse response surface model based on moving Latin hypercube patterns for reliability-based design optimization of ultrahigh strength steel NC milling parameters. *Struct. Multidiscip. O.*, 44(5), 613-628. https://doi.org/10.1007/s00158-011-0672-5

Zhang, S., Fu, B.W. and Sun, L. (2021). Investigation of the jet characteristics and pulse mechanism of self-excited oscillating pulsed jet nozzle. *Processes*, 9(8), 1423-1423. https://doi.org/10.3390/PR9081423

Zhang, Y., Han, Z.H. and Zhang, K.S. (2018). Variable-fidelity expected improvement method for efficient global optimization of expensive functions. *Struct. Multidiscip. O.*, 58(4), 1431-1451. https://doi.org/10.1007/s00158-018-1971-x

Zhou, Z., Ge, Z.L., Lu, Y.Y. and Zhang, X.W. (2017). Experimental study on characteristics of self-excited oscillation pulsed water jet. *J. Vibroeng.*, 19(2), 1345-1357. https://doi.org/10. 21595/jve.2016. 17564